Strong dependency of the tribological behavior of Cu-Zr based bulk metallic glasses on relative humidity in ambient air

Solène Stoens, Paul Laffont, Rémi Daudin, Alexis Lenain, Guillaume Colas, Pierre-Henri Cornuault

Strong dependency of the tribological behavior of Cu-Zr based Bulk Metallic Glasses on relative humidity in ambient air

Solène STOENS[1], Paul LAFFONT[2], Rémi DAUDIN[2], Alexis LENAIN[3], Guillaume COLAS[1], Pierre-Henri CORNUAULT[1]*

[1] *Univ. Bourgogne Franche-Comté FEMTO-ST Institute CNRS/UFC/ENSMM/UTBM, Département de Mécanique Appliquée, Besançon, 25000, France*

[2] *Univ. Grenoble Alpes, CNRS, SIMaP, Grenoble, 38000, France*

[3] *Vulkam Inc. Amorphous metal micro casting / www.vulkam.com / Gières, 38610, France*

* Corresponding author: P-H CORNUAULT, E-mail: pierre-henri.cornuault@ens2m.fr

Abstract: Bulk Metallic Glasses (BMGs) are new competitors to traditional crystalline metals, thanks to their outstanding mechanical properties. However, the tribological response of BMGs is still poorly understood. In the present study, the control of relative humidity (RH) enabled to observe a high repeatability of the friction tests between Cu-Zr based BMG plates and 100Cr6 balls. Interestingly, the wear rate of BMGs is especially low thanks to a 3rd-body tribolayer that forms on the BMG surface, composed of oxidized wear particles originating from the ball. The morphology of this tribolayer is highly correlated to RH.

Keywords: Bulk Metallic Glasses, tribology, oxide transfer layer, relative humidity

1 Introduction

Bulk Metallic Glasses (BMGs) are known for their especially high mechanical properties among which high yield strength and high elastic strain [1]. This explains why BMGs are currently finding more and more applications in different fields including magnetic applications (nanometer-accurate actuators), structural applications (sporting goods, medical implants), optical devices (mirrors), defense and space applications, and micromechanical systems (microgears for micromotors) [2–4]. The last category involves ensuring good surface properties, namely good tribological behavior.

However, the tribological behavior of BMGs remains poorly understood, because of unpredictable wear resistance. Among the few studies that deal with the tribological behavior of BMGs, results and interpretations are in conflict with one another. Many factors do not have an explicit impact on friction and wear of BMGs: mechanical properties of BMGs (hardness specifically) [5–10], contact conditions (normal load, sliding velocity) [7,11–13], relaxation and partial crystallization [9,14–19]. Contrary to most materials, BMGs do not seem to follow Archard's law, that predicts a linear relationship between hardness and wear volume of a material [20]. However, many authors still try to make a connection between BMG wear resistance and their mechanical properties (hardness [5], toughness [8,21], bulk modulus [10]), but no common agreement emerges. This can be explained by the distinctive plastic strain of BMGs, described as homogenous flow at high temperature (near or above Tg) and shear bands mediated plastic deformation at lower temperature [3,4]. This leads to completely different wear mechanisms as compared to their crystalline counterparts. Instead of work-hardening for crystalline structures, several authors highlight a work-softening behavior of BMGs [13,17,22,23], leading to surface softening after friction. Jiang *et al.*[9] tries to make a connection between hardness, free volumes and crack propagation, in order to explain this

work-softening typical behavior of BMGs. The tribological consequences result in subsurface softening after friction, because of shear bands and free volumes creation [17].

Among BMGs, Cu-Zr based are known for the advantageous combination of the high glass forming ability (GFA) of Zr-based BMGs [3,24], coupled with the good mechanical properties of Cu-based BMGs, especially their ductility and strength [24]. Cu-Zr-based BMGs have a proven interest in microgears [21], but there is little detailed understanding of their friction and wear mechanisms. Salehan *et al*.[26] suggested a classification of wear mechanisms of Zr-based BMGs into three categories. 1) microcracks followed by delamination and abrasive wear by detached particles, 2) Shear banding and subsequent work-softening, 3) oxide tribolayer formation and possible peeling-off. The third category introduces a possible contribution of oxide tribolayer in the friction and wear behavior of BMGs, in addition to the mechanical contribution discussed above. Indeed BMGs are known for their higher sensitivity to oxidation than their crystalline counterparts [9,16,27], and a few studies based on AFM measurements deal with the tribological impact of the native oxide present on the surface of BMGs [28–30]. At the macroscale, some tribological studies highlight the formation of an oxide tribolayer that forms during friction [9,13,16,19,24], sometimes resulting from material transfer [11,15,17,22,31,32], leading to the establishment of a 3rd body at the interface. However, oxidation highly depends on the oxidative environments considered, and the effective control of relative humidity (RH) is often lacking in tribological studies. RH is indeed of great importance, as it is known to have a strong impact on the tribology of metals and ceramics [33,34]. In the field of BMGs, very few studies took into account the possible environmental impact on the friction and wear, and the few ones exclusively focus on vacuum, argon and oxygen [23,35,36]. To the best of our knowledge, there is, to the present day, no study dealing with the impact of RH on the tribological behavior of BMGs, this is why the current work aims at investigating their frictional and wear behavior with controlled RH.

2 Materials & Methods

2.1 Sample preparation

The four BMG compositions presented in this study are Cu-Zr based. Two compositions have an equivalent ratio of Cu and Zr ($Cu_{47}Zr_{46}Al_7$ and $Cu_{45}Zr_{46}Al_7Nb_2$, at%) named CuZr and CuZr+Nb, respectively. The two other compositions are rich in Zr ($Zr_{60}Cu_{28}Al_{12}$ and $Zr_{61}Cu_{25}Al_{12}Ti_2$, at%) named Zr and Zr+Ti, respectively.

The BMG samples were produced by arc-melting fragments of each elements of high purity (> 99.9 %) under argon atmosphere. The melting operation was repeated five times to ensure a high chemical homogeneity. The primary alloys obtained were then injected into dedicated moulds to produce plate-shaped samples of $15 \times 10 \times 1$ mm^3. X-rays diffraction measurements were performed to ensure the amorphous structure of each composition, using a X'Pert Pro MPD diffractometer from PANalytical with Cu-Kα radiations (*cf.* Supplementary Material fig. S1). Main mechanical properties of BMG plates are listed in Table 1. Young's modulus were determined using ultrasonic techniques, and Vickers hardness was measured under a load of 1 kg during 10 seconds (means and standard deviations are calculated from 20 measurements within two different samples).

Table 1 - Denomination, composition and mechanical properties of the studied Bulk Metallic Glasses. Asterisk refers to data from the literature [10,32].

	Sample denomination	Composition [at%]	Young's modulus (GPa)	Poisson's ratio	Hardness (HV)	Sa roughness parameter (nm)
Cu-Zr based	CuZr	$Cu_{47}Zr_{46}Al_7$	90	0.36*	480 ± 5	68 ± 4
	CuZr+Nb	$Cu_{45}Zr_{46}Al_7Nb_2$	90	0.36*	485 ± 5	73 ± 2
Zr based	Zr	$Zr_{60}Cu_{28}Al_{12}$	83	0.36*	452 ± 4	75 ± 5
	Zr+Ti	$Zr_{61}Cu_{25}Al_{12}Ti_2$	83	0.36*	453 ± 4	61 ± 2
	Ball	100Cr6	210*	0.29*	805*	97 ± 5

Prior to the friction tests, plates were mechanically polished with sandpapers (until P4000 grad) until a mean Sa roughness parameter close to 70 nm (see Table 1), and then ultrasonically cleaned in high purity propan-2-ol during 3 min at 70°C before being dried in air. Roughness values were determined by variable focus optical microscope (InfiniteFocus, Alicona Imaging GmbH). Means are calculated from three measures performed on 200 × 270 µm² areas.

2.2 Friction tests

Friction tests were performed using an in-house designed ball-on-plate tribometer in dry sliding condition against 5 mm diameter 100Cr6 steel balls of grade 10 quality. 100Cr6 is chosen for its usual use in industrial applications with tribological interest, such as ball bearings. The tribometer achieved reciprocating linear motion with a ± 1 mm displacement stroke at 1 Hz, until a final number of cycles (N) ranging from 200 to 10,000 at a sliding velocity of 4 mm/s. A constant normal force (F_N) of 1 N was applied using dead weight, that corresponds to an initial maximal hertzian contact pressure of 520 MPa and 540 MPa, for Zr-based plates and CuZr-based plates, respectively. A LVDT sensor (Linear Variable Differential Transformer) measured the relative displacement of the ball during the tests (Δh), simultaneously to a piezoelectric sensor that measured the frictional force (F_T). For each friction cycle acquired, the average friction coefficient μ_i was calculated from an energetic point of view using Equation 1, where Δh_0 refers to the distance between the two points of the track corresponding to $F_T = 0$, namely the forward and backward motion (2 mm). After each friction test, a stabilized friction coefficient μ_{stab} is calculated (Equation 2), corresponding to the average of all μ_i from the beginning of μ_i stabilization (with N_{stab} the cycle that corresponds to the start of the steady-state regime) to the end of the test (with N the final number of cycles). $\Delta\mu_i$ refers to the standard deviation of μ_i over the same cycle range (from N_{stab} to N).

$$\mu_i = \frac{1}{2\Delta h_0} \int \frac{|F_T|}{F_N}\, dh \qquad \text{Equation 1}$$

$$\mu_{stab} = \frac{1}{N - N_{stab}} \sum_{i=N_{stab}}^{N} \mu_i$$ Equation 2

All friction tests were performed at room temperature (25 ± 2°C) in air, with a controlled RH ranging from 20 % to 80 % thanks to solutions of sodium hydroxide with variable concentrations, as described in several works [37,38]. The whole tribometer was located in a tightly sealed chamber, and the inner RH was controlled thanks to an external flask of NaOH solution. Air circulation from the flask to the chamber was ensured by a peristaltic pump. A fan located in the closed chamber allowed to homogenize the RH until reaching the desired value, and was turned off before starting friction tests. RH was continuously monitored throughout the test with an ALMEMO® Control Hygrometer.

2.3 Surface analyses

The surface topography of each friction tracks (plates and balls) was characterized by optical means, with a variable focus optical microscope (InfiniteFocus, Alicona Imaging GmbH). The raw 3D surface topography images were processed with the software Gwyddion in order to measure roughness and wear volume, according to the method described by Ayerdi *et al* [39]. First, both plate and ball surfaces were flattened by subtracting analytical surfaces obtained from the least-squares method corresponding either to the analytic closest plane (for plates) or quadratic surface (for balls). Wear volumes were then calculated in reference to the resulting average plane. Through this definition, a positive volume means a loss of matter (*e.g.* ejected particles), and a negative volume means addition of matter (material transfer). The wear rates K ($mm^3.N^{-1}.m^{-1}$) of the plate (K_p) and the ball (K_b) were defined as the wear volume normalized by units of sliding distance and normal force, as described in Equation 3. V_{plate} and V_{ball} represent the wear volumes of the plate and the ball respectively (mm^3), 2 × d the distance covered in one cycle (with d = 2 mm in the actual configuration), N the number of cycles, and F_N the normal force applied (N).

$$K_p = \frac{V_{plate}}{2 \times d \times N_{cycles} \times F_N} \quad \text{and} \quad K_b = \frac{V_{ball}}{2 \times d \times N_{cycles} \times F_N}$$ Equation 3

All wear tracks were also observed by means of optical microscopy (Digital Microscope Keyence VHX-7000). Post-processing of images was performed with the software ImageJ, in order to estimate the 3rd-body coverage of the wear tracks (*cf.* Supplementary Material fig. S2). Scanning Electron Microscopy (SEM) observations were then performed on wear tracks, using a FEI Apreo SEM, equipped with SE detector (secondary electrons) and BSE detector (backscattered electrons), with a beam voltage and beam current of 5 keV and 0.1 nA. Energy Dispersive Spectroscopy (EDS) analyses were conducted at 5 keV with a Bruker SD Detector. A 3D-SEM image combined with EDS cartography was achieved thanks to the software Mountains® from Digital Surf. A FIB cross section was performed using a Zeiss ultra 55 MEG-FEG, through a regular cross section performed at 30 keV and 2.5 nA followed by two successive cleaning cross sections performed at 0.4 nA and 80 pA.

X-rays photoelectron spectroscopy (XPS) analyses were performed on BMG surfaces prior to friction tests (after polishing and cleaning) and after friction tests (localized on wear tracks) with an Al Kα monochromatic excitation source.

3 Results

3.1 XPS analyses on raw surfaces

The XPS analyses carried out on each BMG compositions give information about the chemical elements in presence on the extreme surface, until an approximate depth of 2 nm. The energy of each peak indicates that all the elements are in an oxidized form, namely ZrO_2, Cu_2O, Nb_2O_5, TiO_2 and different aluminum oxides including Al_2O_3 and $Al(OH)_3$ (*cf.* Supplementary Material fig. S3). A semi-quantitative analysis is made possible by the atomic sensitivity factor method [40], whose calculation is based on the area underneath each peak (Table 2). Among all BMG compositions, the major elements in presence are Zr and Al. Surprisingly, Cu is present in negligible proportion as compared to the bulk composition (Table 1). In comparison, both Zr-based (Zr and Zr+Ti) contain more than 60 at% of Zr and less than 2 at% of Cu. Both

Cu-Zr-based (CuZr and CuZr+Nb) contain less Zr (approx. 50 at%) and more Cu (approx. 10 at%). About Al, between 22 at% to 30 at% are detected on all surfaces, much more than in the bulk (7 at% – 12 at%). Microalloyings of Ti (in Zr+Ti) and Nb (in CuZr+Nb) are detected in the same proportion as in the bulk (2 at%). It is assumed that the presence of Si may come from the polishing process.

The results are in good agreement with the literature revealing that a thin oxide film of a few nanometers grows on the surface of most BMGs exposed to ambient conditions [29]. Regarding Cu-Zr based BMGs, several authors show that after annealing, surfaces are enriched in Zr and Al, compared to the Cu rate which drops significantly [41–43] . Most identified oxides are ZrO_2, Al_2O_3 and Cu_2O [41,44]. Kilo *et al*. [43] describes a Cu and Zr dissociation mechanism during oxidation, leading to a Zr-rich layer on the top surface and a Cu-rich layer underneath. This may explain the surprising amount of Zr and Al as compared to Cu.

Table 2 - Quantitative analyses by XPS of the extreme surface of the four alloys after polishing and cleaning in isopropanol (at%). Numbers in brackets refer to the theorical atomic composition of the bulk material.

Composition (at%)	Zr		Cu		Al		Nb		Ti		Si
CuZr	55.7	(46)	9.5	(47)	24.9	(7)	-		-		9.9
CuZr+Nb	46.7	(46)	12.3	(45)	27.8	(7)	2.4	(2)	-		10.8
Zr	63.3	(60)	1.7	(28)	24.3	(12)	-		-		10.6
Zr+Ti	62.1	(61)	1.6	(25)	22.0	(12)	-		2.1	(2)	12.3

3.2 Tribological tests: repeatability survey

Primary tribological tests allowed us to identify whether the frictional behavior of BMGs is repeatable or not in similar conditions of RH, normal force and sliding velocity. Four tests

were carried out at 50 ± 1 %RH, 1 N, during 5,000 cycles. The variations of the friction coefficient for each BMG are displayed on Figure 1a. The variation of the friction coefficient is highly similar between the four tests for each BMG. The running-in-process occurring during the first 2,000 cycles is identical between both Zr-based (Zr and Zr+Ti) and between both Cu-Zr-based (CuZr and CuZr+Nb), but slightly different in between the two BMG categories. The steady-state regime of friction was quickly reached: from 2,000 cycles, μ_i was considered as stable for all tests. The stabilized coefficient of friction μ_{stab} defined in Equation 2, was therefore calculated with $N_{stab} = \frac{2}{5} N$. For instance, the stabilized friction coefficient μ_{stab} calculated for a test of 5,000 cycles is the mean of all friction coefficients μ_i calculated for each cycle between 2,000 to 5,000 cycles (Figure 1a).

The value of μ_{stab} is equal to 0.70 ± 0.02, 0.67 ± 0.03, 0.69 ± 0.04, 0.67 ± 0.03 for CuZr, CuZr+Nb, Zr and Zr+Ti respectively. As far as the RH is kept constant, both the running-in process and μ_{stab} are close enough between identical tests to consider a good repeatability of the tests. Only one test was therefore performed for each parameter combination in the following experiments.

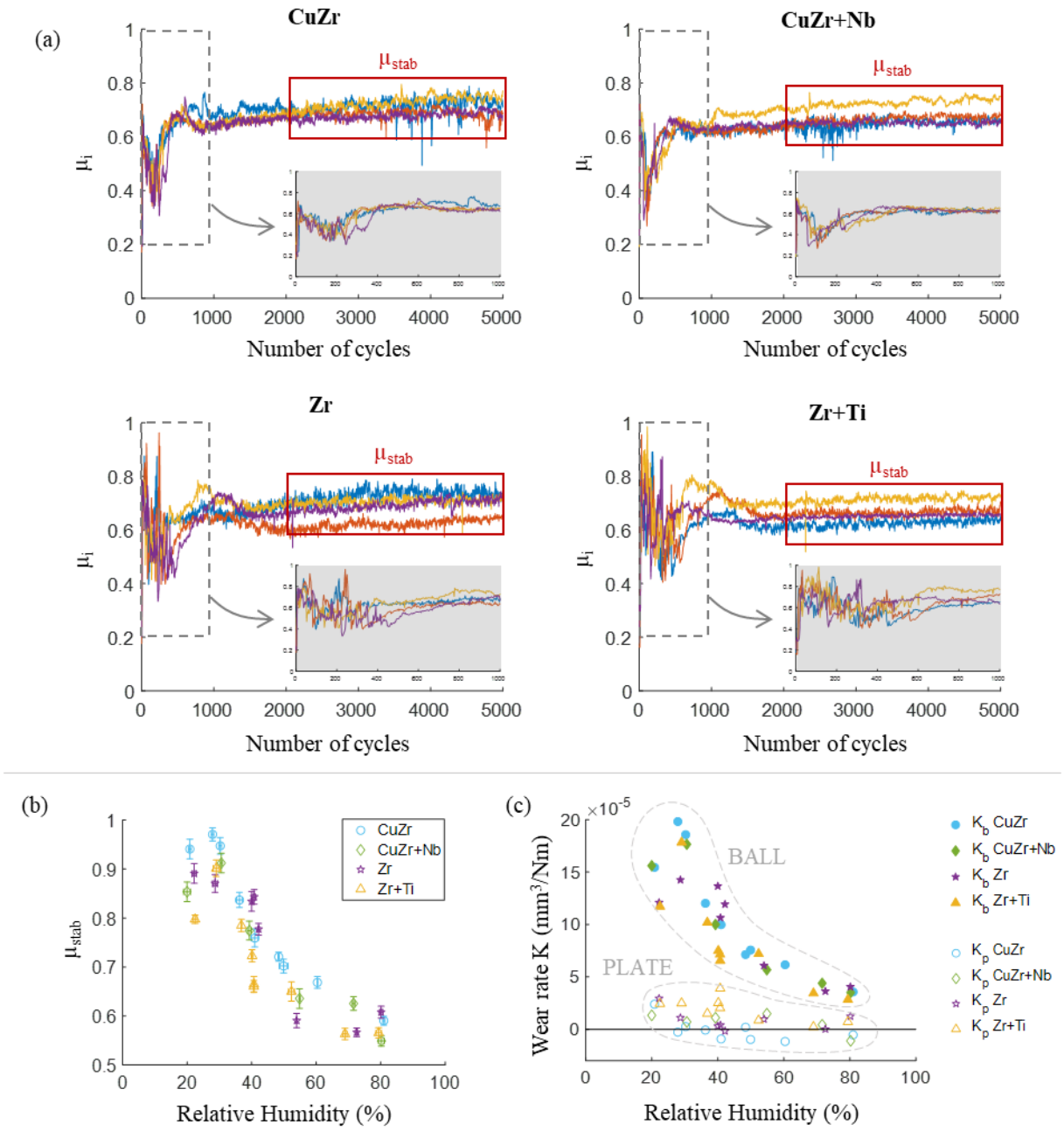

Figure 1 - Repeatability tests performed on the four BMG compositions: friction coefficient μi against the number of cycles (a). RH = 50 ± 1 % and F_N = 1 N. Stabilized friction coefficient versus RH (b), with standard deviation bars associated to $\Delta\mu_i$ (in ordinate) and ΔRH (in abscissa). Wear rates K of plates (unfilled markers) and wear rates K of balls (filled markers) versus RH (c).

3.3 Tribological tests: RH impact

3.3.1 Friction and wear

The investigation of the impact of RH on the tribological behavior of BMGs was carried out on the four alloy compositions. The variation of the friction coefficient, the wear rate of the plate and the wear rate of the ball depending on RH are displayed on Figure 1b and c. A strong dependence of the friction coefficient to RH is highlighted: starting at 0.95 below 30 %RH, the friction coefficient quickly decreases with increasing RH down to 0.55 at 80 %RH. This variation is similar whatever the chemical composition of the alloy. Regarding the wear rates, BMG plates show a high wear resistance with wear rates ranging from -2.10^{-5} to 5.10^{-5} mm^3/Nm. Most of the values keep close to zero, and some are even negative, meaning that material transfer from the ball to the plate occurred. This is consistent with the wear rates of the ball, that is up to 10 times higher than the wear rates of the plate. The wear rate of balls strongly depends on RH: K_b gets lower and lower when increasing RH.

3.3.2 Morphology and composition of wear tracks

Figure 2a displays optical images of Zr+Ti wear tracks after friction tests performed at 80 %RH and 20 %RH. Observations emphasize the presence of a 3rd body at the contact interface. At 80 %RH, the wear track on the plate is thin and covered with expanded and smooth patches that lay on the surface, with lots of small particles distributed around the patches (Figure 2c). At 20 %RH, the wear track is larger and covered with a homogeneous repartition of small and rough patches. Two profiles extracted from those tracks (Figure 2b) show that at 80 %RH the expanded and smooth patches are above the mean surface height, contrary to the island-shaped patches at 20 %RH that are above but also below the mean surface height. Conversely, the wear tracks of all the balls have the shape of a regular disc, without any 3rd body on the surface (*cf.* Supplementary Material fig. S4). Wear particles are present outside of the track.

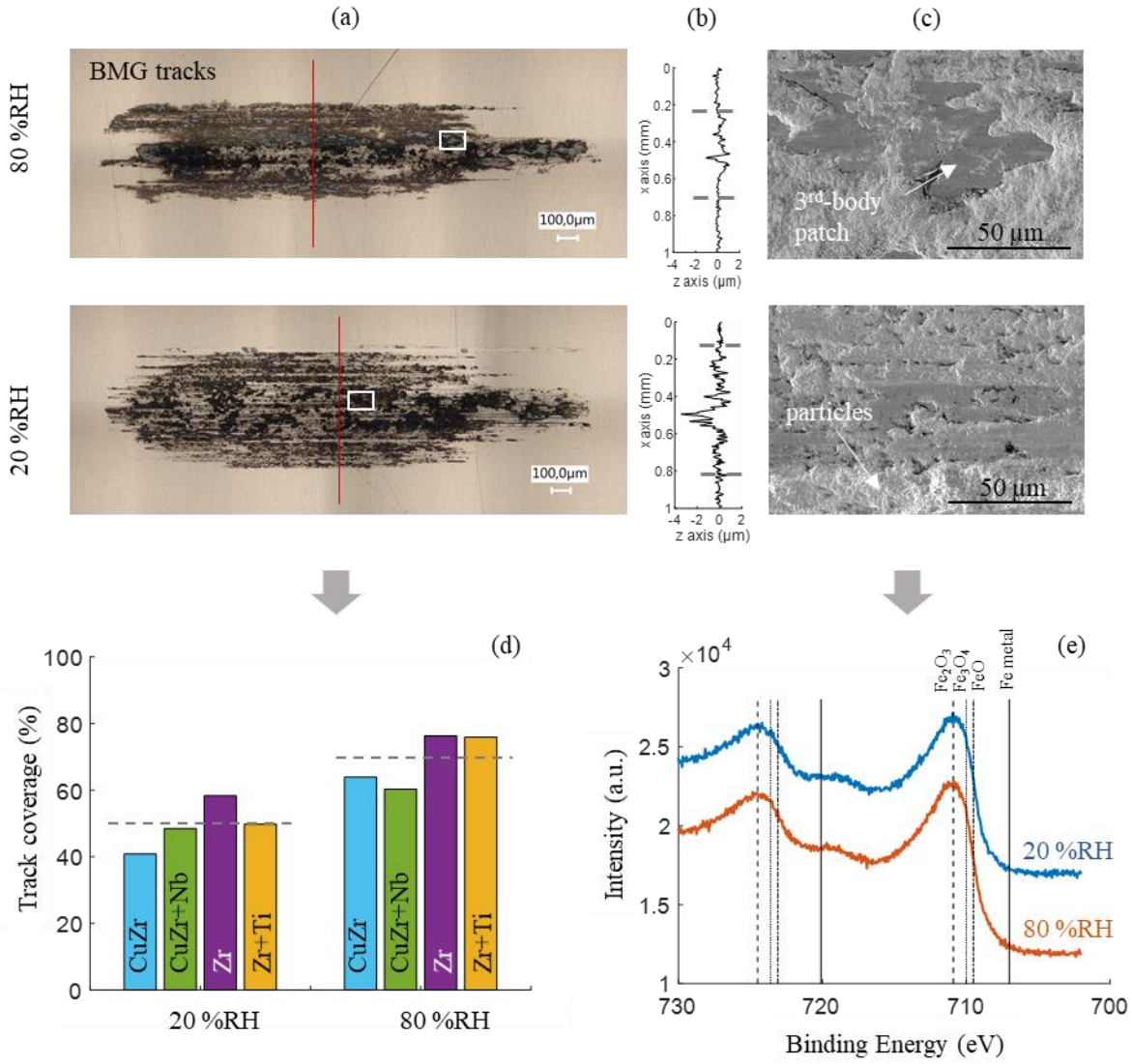

Figure 2 - Optical images of Zr+Ti wear tracks after friction tests at 80 %RH and 20 %RH (a). Height profiles along the red lines at 80 %RH and 20 %RH (b). Dashed lines represent the boundaries of the wear track. SEM pictures (SE detector) of the white-framed zones at 80 %RH and 20 %RH (c). 3rd body coverage over the wear tracks at 20 %RH and 80 %RH for each alloy composition (d). Dashed lines represent the average coverage at 20 %RH and 80 %RH. Fe2p peak from XPS analyses performed on CuZr wear tracks after friction tests at 20 %RH (blue) and 80 %RH (red) (e). Solid lines refer to the theorical peaks of Fe metal, dash-dotted lines refer to FeO, dashed lines refer to Fe_2O_3 and dotted lines to Fe_3O_4 [45].

SEM observations with a BSE detector allowed the identification of two types of 3rd body patches: most of the track is covered by dark patches, but a few white patches can be found in some localized areas (*cf.* Supplementary Material fig. S5). Indeed, the BSE detector enables to differentiate the light elements (*i.e.* low atomic number Z) and the heavy elements (*i.e.* high Z), leading to a grey scale correlated to the elemental composition: heavier elements appear bright compared to lighter elements. The elemental composition of 3rd body patches was studied by EDS analyses. Dark patches are mostly composed of Fe and O, contrary to white patches that are composed of Cu, Zr, Al and O (*cf.* Supplementary Material fig. S5c). This suggests that most of the 3rd body patches come from oxidized wear debris of the ball (Fe-oxides), and a few patches come from oxidized wear debris of the BMG (Zr-Cu-Al-oxides). Two different structures of 3rd-body patches are observed: either the superposition of Fe-oxides that spread over Zr-Cu-Al-oxides that can reach 3 µm-high (*cf.* Supplementary Material fig. S5), or a mixed dark-white patch in zebra stripes, perpendicularly to the sliding direction (Figure 3b), corresponding alternatively to Zr-Cu-Al-oxides and Fe oxides (*cf.* Supplementary Material fig. S6). A FIB cross section displayed on Figure 3c was performed on one of these zebra striped 3rd-bodies. The stripes extend beneath the surface until a depth superior to 1 µm, and their morphology suggests a very high plastic deformation and surface ductility. There are porosities at the root of some stripes, and the greyscale contrast along the stripes exhibits a complex composite structure of Fe-oxides and Zr-Cu-Al-oxides (Figure 3d).

However, there are only few Zr-Cu-Al-oxide patches, and most of the 3rd-body layer is composed of dark-appearing Fe-oxides patches. XPS analyses performed over the friction tracks of CuZr samples resulting from tests at 20 %RH and 80 %RH are displayed on Figure 2e. The Fe $2p_{3/2}$ peak positions at 20 %RH and 80 %RH are 710.8 eV and 710.9 eV respectively. This corresponds to Fe_2O_3 oxides, according to the theorical binding energy of

Fe_2O_3 $2p_{3/2}$ peak at 710.9 eV [45]. This shows that the nature of iron oxide formed remains the same from 20 %RH to 80 %RH.

The BSE detector enables to differentiate the 3rd-body layer from the BMG raw surface, because of the strong proportion of Fe-oxides constituting the 3rd-body as compared to the Zr-Cu-Al BMG raw surface, responsible for a sharp grey-level contrast (*cf*. Supplementary Material fig. S2). Thanks to image binarization of SEM observations, a 3rd body coverage was estimated for each track at 20 %RH and 80 %RH (Figure 2d). The coverage ratio was calculated on the whole central part of the wear track deprived of its extremities. Figure 2d confirms that at 20 %RH, the 3rd body coverage of wear tracks is smaller (49 % in average) than at 80 %RH (69 % in average).

The combination of XPS analyses and wear coverage shows that humidity only affects the track coverage and morphology of the 3rd body, but not its chemical nature (*cf*. Figure 2c, d and e).

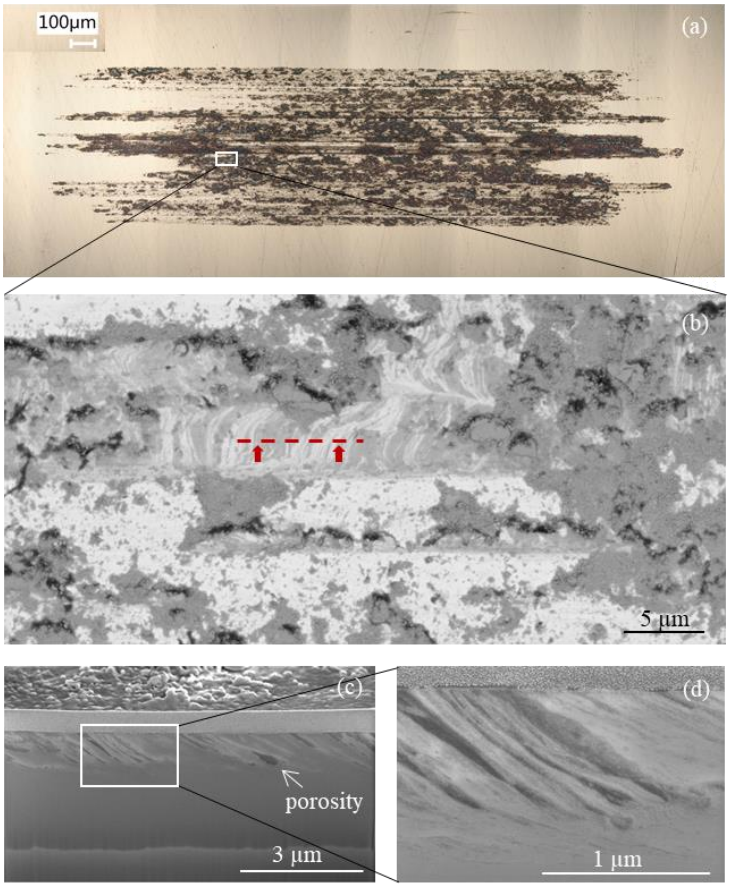

Figure 3 – Optical image of a CuZr+Nb wear track at 20 %RH (a) and MEB observation (BSE) associated to the white-framed zone (b). FIB cross section performed along the red dashed line (c and d).

3.4 Tribological tests: increasing number of cycles

3.4.1 Friction and wear

In order to understand the wear mechanism of Cu-Zr-based BMG and more specifically the 3rd-body-formation scenario, a tribological study with increasing number of cycles was performed**,** with one test performed with each following number of cycles (N): 200 – 350 – 500 – 750 – 1,000 – 1,500 – 2,000 – 3,500 – 5,000 – 10,000. The μ_i superposition between each test is displayed on figure S7 of Supplementary Material. The RH chosen for this study was 50 %RH for three reasons: 1) The nature of the 3rd-body does not change with varying RH, 2) 50% RH corresponds to a medium humidity in ambient conditions and 3) the stabilization of

RH is easier and faster to obtain. Two BMG compositions were selected, namely Zr and CuZr, because of the close tribological behavior exhibited by CuZr and CuZr+Nb, and on the other hand by Zr and Zr+Ti (see Figure 1a). The variation of friction coefficient and wear rates of the ball and the plate against the number of friction cycles are displayed on Figure 4, for both Zr and CuZr.

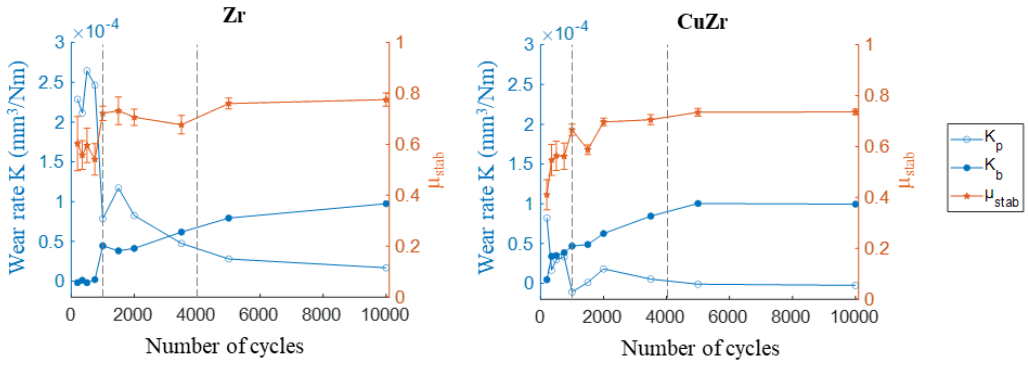

Figure 4 - μ_{stab} (red stars), K_p (unfilled circles) and K_b (filled circles) against the number of friction cycles. Each point refers to a single test. Standard deviation bars are associated to $\Delta\mu_i$. Tests were performed at 50 ± 1 %RH for both Zr (left) and CuZr plates (right).

Sliding can be described according to three successive stages:

1) From sliding initiation to 1,000 friction cycles, μ_{stab} fluctuates, and the BMG plate experiences severe wear, especially Zr. μ is highly reproductible from test to test (*cf.* Supplementary Material fig. S7).
2) From 1,000 to 4,000 friction cycles, the ball wear rate suddenly increases contrary to the BMG wear that decreases, until a reversal. The standard deviation of μ_{stab} decreases progressively while μ_{stab} is reaching a stable value.
3) From 4,000 to 10,000 friction cycles, a stabilized value is reached for μ_{stab} and the wear rates of both the plate and the ball. The standard deviation of μ_{stab} reaches very low values.

3.4.2 Morphology of wear tracks

SEM observations carried out on the wear tracks are displayed on Figure 5. The track becomes larger as the number of cycles increases. First, a ploughing striation is created in the middle of the track, followed by other secondary striations when increasing the number of cycles. At the extremities and inside of each striation, white 3rd-body patches composed of Zr-Cu-Al-oxides are formed (*cf*. Supplementary Material fig. S8a). Beside and between these striations, several 3rd body patches are formed by agglomeration of small wear debris mainly composed of iron oxides, that appear darker on BSE pictures. After more than 4,000 cycles, most of the central part of the track is covered by these dark 3rd body patches and no white patches are seen. At each extremities of the tracks, only one white patch is still present, positioned in the middle of the facing contact area of the ball (*cf*. Supplementary Material fig. S8c).

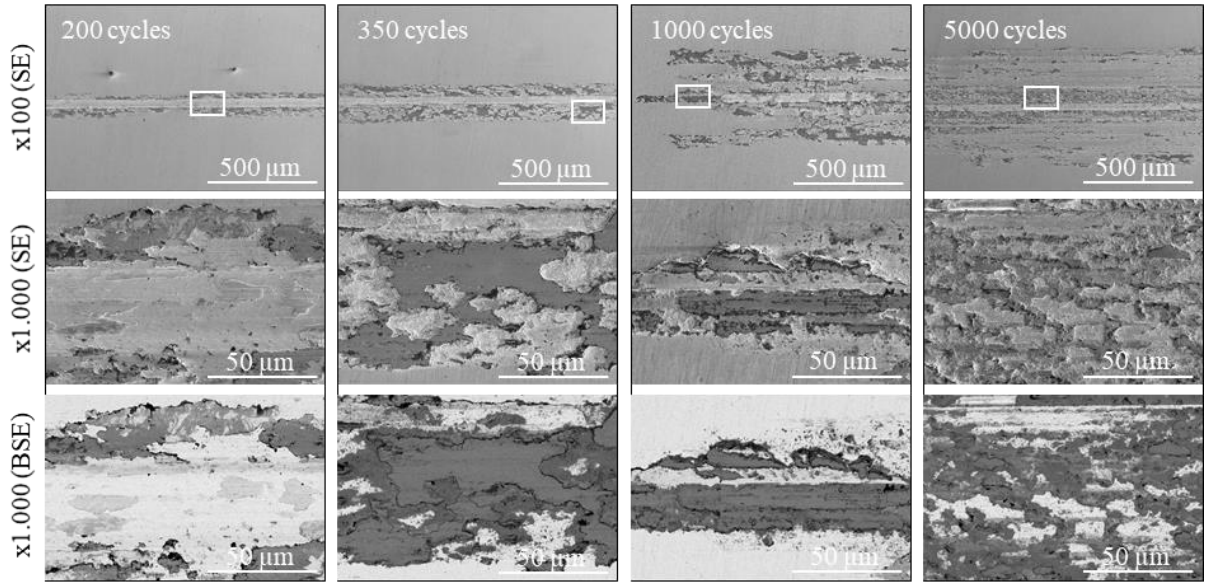

Figure 5 – SEM observations of wear tracks on the CuZr plate after 200, 350, 1,000 and 5,000 friction cycles at 50 %RH (SE detector). Images below correspond to a 10 times higher magnification of the white-framed areas, with both SE and BSE detectors.

4 Discussion

In the literature, most oxide tribolayers formed on BMGs are composed of the elements constituting the BMG. Jiang *et al*. [9], Aditya *et al*. [19], and Wu *et al*. [24] studied the tribological behavior of Zr-Cu based BMGs under ball-on-plate reciprocating sliding against 100Cr6, WC and Si_3N_4 counterparts, respectively. Wang *et al*. [13] studied a Zr-Cu based BMG under pin-on-disk configuration against a GCr6 steel counterpart. All these works describe a tribolayer adhering to the BMG surface composed of oxidized elements of the BMG. For instance, Jiang *et al*. [9] observed the formation of an oxide-based layer when testing $Zr_{52.5}Cu_{17.9}Ni_{14.6}Al_{10}Ti_5$ against 100Cr6. Wear scars were described into two distinct regions: abrasion regions and adhesion regions covered by dark patches. Contrary to the present work, dark patches were exclusively composed of oxidized elements of the BMG, and no iron oxides were detected. A similar BMG sample was thermally and mechanically treated until a crystalline state, and no oxide layer was observed after friction tests. Oxidative wear is thus believed to be one of the predominant wear mechanisms of amorphous metallic alloys. On the other hand, Zhao *et al*. [15], Wu *et al*. [17] and Wu *et al*. [22] described a material transfer from the BMG to the counterface by adhesive wear, under pin-on-disk friction tests between Zr-Cu based BMGs and steel (unspecified), bearing steel and stainless steel, respectively. In all of these situations, BMGs experience a severe wear through particles generation and the formation of a tribolayer composed of the BMG elements. More rarely, material transfer from the counterface to the BMG surface occurs, but only in specific cases such as: 1) the counterface is softer than the BMG [6] , 2) material transfer concerns only the carbon present in the counterface, that mixes with BMG oxides [11], 3) material transfer of Fe occurs when Fe is already present in the BMG composition [31,46]. To the best of our knowledge, only one study deals with the formation of a similar tribolayer as observed in the present study, composed of the particles of the harder steel counterpart, and which form a protective layer over the BMG

surface. Indeed, Cornuault *et al.*[32] observed a comparable tribolayer when testing $Zr_{52.5}Cu_{17.9}Ni_{14.6}Al_{10}Ti_5$ against 100Cr6 with similar contact conditions (reciprocating sliding at 4 mm/s, during 10,000 cycles of ± 1 mm, in ambient air, at 680 MPa of initial maximal hertzian pressure).

Figure 1b highlights the strong dependence to RH during friction of the couple Cu-Zr-based BMGs / 100Cr6. This impact of RH is made visible when looking at the contact interface: the morphologies of patches and 3rd body coverage of the BMG tracks change depending on RH. However, this morphological change is not supported by a chemical change of the oxides formed, which remain Fe_2O_3 whatever the RH. This means that RH does not affect the chemical nature of the oxide particles, but the agglomeration of steel ball debris responsible of the 3rd-body patches aggregation. According to Leheup and Pendlebury [47], a higher RH would act as inhibitor for surfaces oxidation, despite the common thought that presupposes an increase of oxidation in wet environment. Indeed, the oxidative process (induced by O_2 presence) is slowed down because of the presence of other molecules in the surrounding atmosphere (H_2O). This phenomenon should lead to an increase of friction coefficient, in opposition to the present results. De Baets *et al*. [48] observed the same dependency to RH between two steels (bearing steel ball and cold-down steel), with a decrease of the friction coefficient from 0.78 at 20 %RH to 0.60 at 90 %RH. They concluded that the influence of RH was not due to oxidation inhibition, but to boundary lubrication of contacting surfaces. They defined three possible mechanisms to explain this lubricating effect of RH. 1) A change of oxide nature can occur: at low RH, fretting mainly leads to the formation of Fe_2O_3, that can be inhibited at higher humidities, promoting other types of oxidation reactions. 2) Gas adsorption can occur between a molecule and the metal surface, forming a physisorbed layer that lubricates the contact. 3) Condensation of the moisture can happen at very high RH, forming a lubricant film. In the present study, both the second and the third mechanisms might be involved, i.e. physisorbed gas molecules and

condensed water film between the two surfaces. Moreover, Fe_2O_3 is known to have high capability of water adsorption: Yamamoto *et al*.[49] demonstrates the increasing molecular adsorption of water on Fe_2O_3 with increasing RH up to a water coverage superior to 1,5 monolayers. In addition to the lubricant film at the interface, physisorbed water may be present around the wear particles coming from the ball (Fe_2O_3), therefore an enhanced agglomeration of particles to form layer patches is observed at high RH.

Tests performed with increasing number of friction cycles enables to describe the wear scenario into three successive stages, schematized on Figure 6.

During the first stage, the hard steel ball creates a first ploughing striation on the softer BMG surface. Wear debris produced during this abrasion process are originating from the native oxide present on the extreme surface, mainly composed of ZrO_2, aluminum oxides (Al_2O_3 and $Al(OH)_3$) and Cu_2O, according to the XPS analyses (*cf*. Supplementary Material fig. S3). These oxidized particles are compacted and flattened into small patches adhering to the surface of the BMG. The newly exposed surface inside the ploughing striations is probably Cu-enriched according to the dissociation mechanism described by Kilo et al.[43], with a Cu-rich layer underneath the upper Zr-rich layer. This ploughing mechanism associated to the formation of Zr-Cu-Al-oxide patches can explain the high BMG wear volume and the fluctuating friction coefficient during this early stage of friction. These oxides are known to be hard and abrasive, especially ZrO_2 and Al_2O_3 [50]. Consequently, the abrasive mechanism gradually reverses: the Zr-Cu-Al-oxides become responsible of the progressive abrasion of the steel ball, leading to the production of iron oxides (Fe_2O_3) particles in the contact interface.

During the second stage, Fe_2O_3 particles are compacted into patches and get anchored inside the wear track through three distinct processes: 1) Fe-oxide patches adhere to the previously formed Zr-Cu-Al-oxide patches and cover them entirely or partially. 2) Fe_2O_3 get anchored into some cracks on the surface of Zr-Cu-Al-oxide patches. Indeed, adhesion between

steel ball and BMG plate may induce some apertures in which iron oxides are trapped. Then, the successive forward and backward motions promote strain in elongation resulting into the observed stripe shape. 3) Fe-oxide patches adhere directly to the worn surface of the BMG. As a common prerequisite to these three adhesive mechanisms, the prior presence of Zr-Cu-Al-oxide patches is necessary to play an anchoring role of Fe_2O_3 patches. The spontaneous adhesion of Fe_2O_3 particles to the BMG surface could be explained by the chemical affinity between Fe and Zr / Al (heat of mixing Fe-Zr = -25 kJ/mol ; Fe-Al = -11 kJ/mol)[31]. The wear mechanism described in this study depends on the chemical reactivity of elements Zr-Cu-Al and Fe.

Finally, the third stage corresponds to a steady-state establishment. The tribolayer is on the one hand responsible of an increase of the wear of the steel ball because particles are detached from the ball, and on the other hand a decrease of the BMG wear, thanks to the protective tribolayer that is being formed from those iron oxide particles. However, this steady state is dependent to RH. At low RH, the wide track is covered by small and rough 3rd-body patches, constituting a highly abrasive surface. The facing ball undergoes severe wear and much iron-oxide particles are produced, that subsequently leave the contact area. At high RH, the high water adsorption on Fe_2O_3 leads to the agglomeration of particles into large and smooth 3rd-body patches. Additionally, a lubricant film of water molecules may also contribute to the smaller friction coefficient and wear rates.

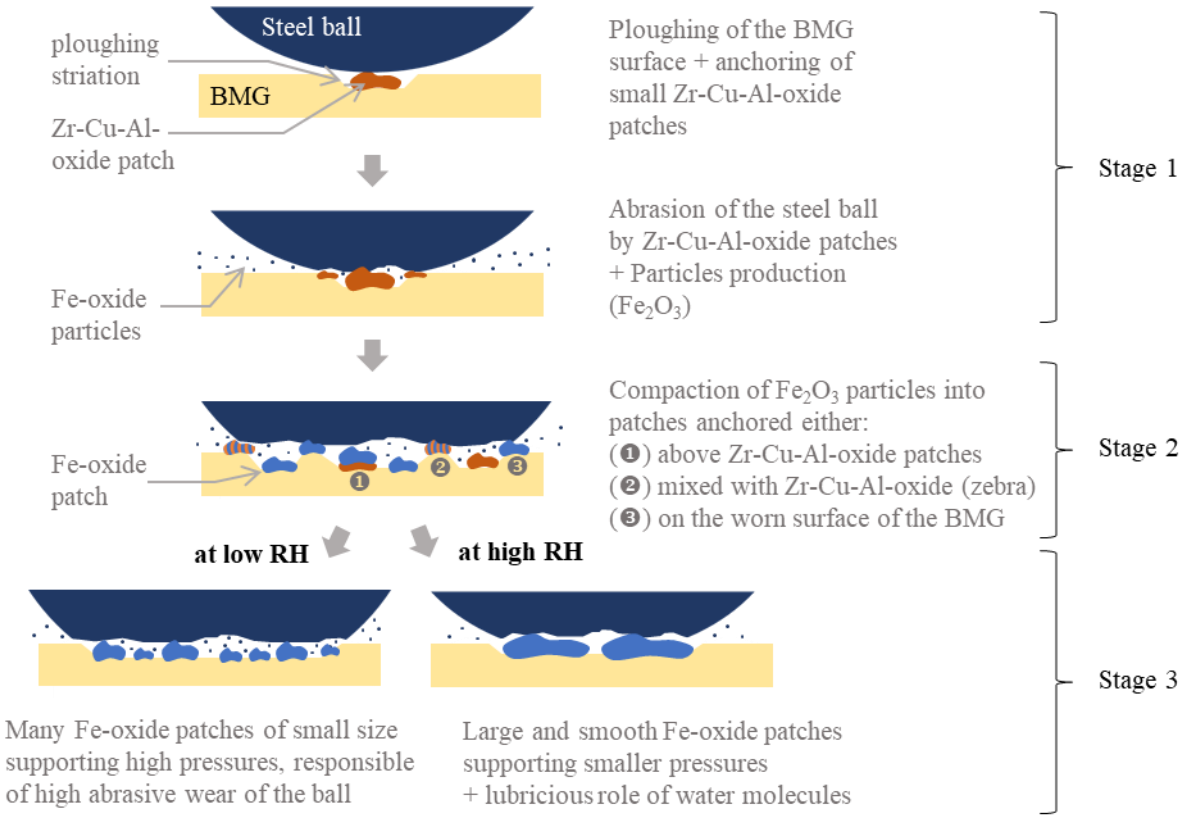

Figure 6 - Scheme of the three successive stages of wear mechanisms involved between Cu-Zr-based plates and 100Cr6 balls.

The newly formed interface, after the steady state establishment, is composed of steel (ball) against iron oxides (plate). This is therefore comparable to steel against steel tribological studies with varying humidities. Klaffke *et al*. [51] studied the tribological contact between two 100Cr6 specimens through fretting tests, and the friction coefficient follows exactly the same tendency as in the present study (*cf*. Figure 7). Oh *et al*. [52] also obtained similar results with carbon steels (1020, 1040 and 1045). The behavior is described as severe wear at low RH (because of adhesive wear in metal-metal contact) to soft wear at high RH (because of oxides presence and water adsorption). This shows that the tribological behavior of the BMG is strongly correlated to the counterpart material. As mentioned above, the wear mechanism described in this study is firstly due to the formation of Zr-Cu-Al-oxide patches formed from the native oxide present on BMG surfaces, playing afterwards an anchoring site for Fe_2O_3

particles detached from the ball. These Fe-oxide patches protect the BMG from subsequent wear, although 100Cr6 steel is harder than the BMG.

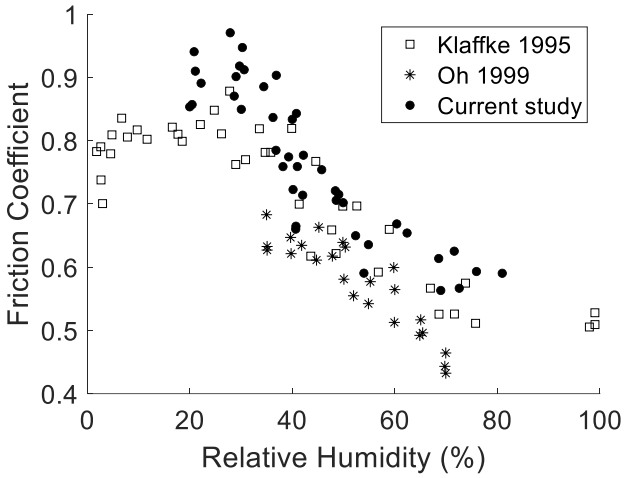

Figure 7 – Friction coefficient depending on RH of the present study (dots), compared to the results obtained in two different studies: 100Cr6 against 100Cr6 [51] (squares) and carbon steels 1020 1041 and 1045 against themselves [52] (stars).

5 Conclusion

Until the present day, the literature about BMGs shows an erratic behavior in their tribological response. This study is a first step towards a reproducibility of the tribological response, as long as the relative humidity (RH) is controlled in addition to the usual contact conditions (normal force, sliding distance and sliding velocity).

Contrary to crystalline metals for which hardness is a determinant parameter, the relationship between hardness and the tribological behavior of BMGs is debatable. Indeed, this work highlights a surprising wear resistance of Cu-Zr-based BMGs provided by a 3rd-body tribolayer composed of Fe_2O_3 oxides coming from the facing 100Cr6 ball. Consequently, the BMG gets a protection despite the higher hardness of the facing counterpart: the 3rd-body patches accommodate friction and protect the BMG substrate from wear. This anchoring

process of Fe_2O_3 patches is made possible thanks to an intermediate formation of Zr-Cu-Al-oxide patches composed of the native oxide of BMGs.

The results show a strong influence of RH on the friction and wear of BMGs and 100Cr6. Indeed, the compaction morphology of iron oxides differs depending on RH. In dry environment, much debris are ejected from the contact and few are compacted into small patches that plays a role of hard asperities responsible of severe wear of the hard ball. In wet environment, because of the probable presence of physisorbed water molecules and condensed water film, much debris gather and compact into large and smooth 3rd-body patches, that can reach 3 µm high.

While rarely questioned in the literature, this study highlights the importance of the chosen counterpart on the tribological behavior of BMGs. In this study, the 100Cr6 counterpart is driving the tribological response after a BMG-dependent running-in period. It might be questioned on whether another steel counterpart would lead to the same behavior. This would have to be addressed in future works.

Acknowledgements

This work was supported by the EUR EIPHI Graduate School (contact ANR-17-EURE-0002). The authors are thankful for the financial support provided by the French National Research Agency (ANR) through the contract ANR-19-CE08-0015. The authors would like to thank Paul Laffont (from SiMAP lab at Univ. Grenoble Alpes, France) for performing the XRD and mechanical properties measurements of the BMGs (Young's modulus and hardness), Olivier Heintz and Anna Krystianiak (from ICB lab at Univ. Bourgogne Franche-Comté, France) for providing the XPS spectrums, Marina Raschetti (from Femto-ST Institute, France) for her help in using Mountains® from Digital Surf, and the technology center MIMENTO (Femto-ST Institute, France).

Supplementary Material: Supplementary material displaying additional figures is available in the online version of this article.

References

[1] A. Inoue, Bulk Glassy Alloys: Historical Development and Current Research, Engineering. 1 (2015) 185–191. https://doi.org/10.15302/J-ENG-2015038.

[2] A. Inoue, N. Nishiyama, New Bulk Metallic Glasses for Applications as Magnetic-Sensing, Chemical, and Structural Materials, MRS Bull. 32 (2007) 651–658. https://doi.org/10.1557/mrs2007.128.

[3] M. Telford, The case for bulk metallic glass, Mater. Today. 7 (2004) 36–43. https://doi.org/10.1016/S1369-7021(04)00124-5.

[4] A.L. Greer, Metallic glasses…on the threshold, Mater. Today. 12 (2009) 14–22. https://doi.org/10.1016/S1369-7021(09)70037-9.

[5] A.L. Greer, K.L. Rutherford, I.M. Hutchings, Wear resistance of amorphous alloys and related materials, Int. Mater. Rev. 47 (2002) 87–112. https://doi.org/10.1179/095066001225001067.

[6] E. Fleury, S.M. Lee, H.S. Ahn, W.T. Kim, D.H. Kim, Tribological properties of bulk metallic glasses, Mater. Sci. Eng. A. 375–377 (2004) 276–279. https://doi.org/10.1016/j.msea.2003.10.065.

[7] B. Prakash, Abrasive wear behaviour of Fe, Co and Ni based metallic glasses, Wear. 258 (2005) 217–224. https://doi.org/10.1016/j.wear.2004.09.010.

[8] D.R. Maddala, R.J. Hebert, Sliding wear behavior of Fe50−xCr15Mo14C15B6Erx (x=0, 1, 2at%) bulk metallic glass, Wear. 294–295 (2012) 246–256. https://doi.org/10.1016/j.wear.2012.06.007.

[9] F. Jiang, J. Qu, G. Fan, W. Jiang, D. Qiao, M.W. Freels, P.K. Liaw, H. Choo, Tribological Studies of a Zr-Based Glass-Forming Alloy with Different States, Adv. Eng. Mater. 11 (2009) 925–931. https://doi.org/10.1002/adem.200900184.

[10] Z. Liao, N. Hua, W. Chen, Y. Huang, T. Zhang, Correlations between the wear resistance and properties of bulk metallic glasses, Intermetallics. 93 (2018) 290–298. https://doi.org/10.1016/j.intermet.2017.10.008.

[11] Z. Parlar, M. Bakkal, A.J. Shih, Sliding tribological characteristics of Zr-based bulk metallic glass, Intermetallics. 16 (2008) 34–41. https://doi.org/10.1016/j.intermet.2007.07.011.

[12] H. Zhong, J. Chen, L. Dai, Y. Yue, Z. Zhang, X. Zhang, M. Ma, R. Liu, Tribological behaviors of Zr-based bulk metallic glass versus Zr-based bulk metallic glass under relative heavy loads, Intermetallics. 65 (2015) 88–93. https://doi.org/10.1016/j.intermet.2015.06.002.

[13] Y. Wang, L. Zhang, T. Wang, X.D. Hui, W. Chen, C.F. Feng, Effect of sliding velocity on the transition of wear mechanism in (Zr,Cu)95Al5 bulk metallic glass, Tribol. Int. 101 (2016) 141–151. https://doi.org/10.1016/j.triboint.2015.11.012.

[14] J. Bhatt, S. Kumar, C. Dong, B.S. Murty, Tribological behaviour of Cu60Zr30Ti10 bulk metallic glass, Mater. Sci. Eng. A. 458 (2007) 290–294. https://doi.org/10.1016/j.msea.2006.12.060.

[15] J. Zhao, M. Gao, M. Ma, X. Cao, Y. He, W. Wang, J. Luo, Influence of annealing on the tribological properties of Zr-based bulk metallic glass, J. Non-Cryst. Solids. 481 (2018) 94–97. https://doi.org/10.1016/j.jnoncrysol.2017.10.033.

[16] H.W. Jin, R. Ayer, J.Y. Koo, R. Raghavan, U. Ramamurty, Reciprocating wear mechanisms in a Zr-based bulk metallic glass, J. Mater. Res. 22 (2007) 264–273. https://doi.org/10.1557/jmr.2007.0048.
[17] X.F. Wu, G.A. Zhang, F.F. Wu, Wear behaviour of Zr-based in situ bulk metallic glass matrix composites, Bull. Mater. Sci. 39 (2016) 703–709. https://doi.org/10.1007/s12034-016-1187-x.
[18] Y. Liu, Z. Yitian, L. Xuekun, Z. Liu, Wear behavior of a Zr-based bulk metallic glass and its composites, J. Alloys Compd. 503 (2010) 138–144. https://doi.org/10.1016/j.jallcom.2010.04.217.
[19] A. Aditya, H. Felix Wu, H. Arora, S. Mukherjee, Amorphous Metallic Alloys: Pathways for Enhanced Wear and Corrosion Resistance, JOM. 69 (2017) 2150–2155. https://doi.org/10.1007/s11837-017-2384-9.
[20] J.F. Archard, Contact and Rubbing of Flat Surfaces, J. Appl. Phys. 24 (1953) 981–988. https://doi.org/10.1063/1.1721448.
[21] D.C. Hofmann, L.M. Andersen, J. Kolodziejska, S.N. Roberts, J.-P. Borgonia, W.L. Johnson, K.S. Vecchio, A. Kennett, Optimizing Bulk Metallic Glasses for Robust, Highly Wear-Resistant Gears, Adv. Eng. Mater. 19 (2017) 1600541. https://doi.org/10.1002/adem.201600541.
[22] H. Wu, I. Baker, Y. Liu, X. Wu, P.R. Munroe, J. Zhang, Tribological studies of a Zr-based bulk metallic glass, Intermetallics. 35 (2013) 25–32. https://doi.org/10.1016/j.intermet.2012.11.010.
[23] X.-Y. Fu, T. Kasai, M.L. Falk, D.A. Rigney, Sliding behavior of metallic glass: Part I. Experimental investigations, Wear. 250 (2001) 409–419. https://doi.org/10.1016/S0043-1648(01)00605-6.
[24] K. Wu, L. Zheng, H. Zhang, Research on high-Al Cu-Zr-Al-Y bulk metallic glass and its composites, J. Alloys Compd. 770 (2019) 1029–1037. https://doi.org/10.1016/j.jallcom.2018.08.130.
[25] L.M. Andersen, Toughness of Wear-Resistant Cu-Zr-Based Bulk Metallic Glasses, 2016. https://ui.adsabs.harvard.edu/abs/2016PhDT.....87A (accessed November 22, 2021).
[26] R. Salehan, H.R. Shahverdi, R. Miresmaeili, Effects of annealing on the tribological behavior of Zr60Cu10Al15Ni15 bulk metallic glass, J. Non-Cryst. Solids. 517 (2019) 127–136. https://doi.org/10.1016/j.jnoncrysol.2019.05.013.
[27] W. Kai, H.H. Hsieh, T.G. Nieh, Y. Kawamura, Oxidation behavior of a Zr–Cu–Al–Ni amorphous alloy in air at 300–425 °C, Intermetallics. 10 (2002) 1265–1270. https://doi.org/10.1016/S0966-9795(02)00163-2.
[28] H. Ma, R. Bennewitz, Nanoscale friction and growth of surface oxides on a metallic glass under electrochemical polarization, Tribol. Int. 158 (2021) 106925. https://doi.org/10.1016/j.triboint.2021.106925.
[29] S.J. Kang, K.T. Rittgen, S.G. Kwan, H.W. Park, R. Bennewitz, Importance of surface oxide for the tribology of a Zr-based metallic glass, Friction. 5 (2017) 115–122. https://doi.org/10.1007/s40544-017-0149-7.
[30] A. Caron, P. Sharma, A. Shluger, H.-J. Fecht, D.V. Louzguine-Luzguin, A. Inoue, Effect of surface oxidation on the nm-scale wear behavior of a metallic glass, J. Appl. Phys. 109 (2011) 083515. https://doi.org/10.1063/1.3573778.
[31] Q. Zhou, W. Han, D. Luo, Y. Du, J. Xie, X.-Z. Wang, Q. Zou, X. Zhao, H. Wang, B.D. Beake, Mechanical and tribological properties of Zr–Cu–Ni–Al bulk metallic glasses with dual-phase structure, Wear. 474–475 (2021) 203880. https://doi.org/10.1016/j.wear.2021.203880.

[32] P.-H. Cornuault, G. Colas, A. Lenain, R. Daudin, S. Gravier, On the diversity of accommodation mechanisms in the tribology of Bulk Metallic Glasses, Tribol. Int. 141 (2020) 105957. https://doi.org/10.1016/j.triboint.2019.105957.
[33] J.K. Lancaster, A review of the influence of environmental humidity and water on friction, lubrication and wear, Tribol. Int. 23 (1990) 371–389. https://doi.org/10.1016/0301-679X(90)90053-R.
[34] Z. Chen, X. He, C. Xiao, S.H. Kim, Effect of Humidity on Friction and Wear—A Critical Review, Lubricants. 6 (2018) 74. https://doi.org/10.3390/lubricants6030074.
[35] H. Wu, I. Baker, Y. Liu, X. Wu, P.R. Munroe, Effects of environment on the sliding tribological behaviors of Zr-based bulk metallic glass, Intermetallics. 25 (2012) 115–125. https://doi.org/10.1016/j.intermet.2011.12.025.
[36] M.R. Jones, A.B. Kustas, P. Lu, M. Chandross, N. Argibay, Environment-Dependent Tribological Properties of Bulk Metallic Glasses, Tribol. Lett. 68 (2020) 123. https://doi.org/10.1007/s11249-020-01364-z.
[37] D.S. Madge, The Control of Relative Humidity with Aqueous Solutions of Sodium Hydroxide, Entomol. Exp. Appl. 4 (1961) 143–147. https://doi.org/10.1111/j.1570-7458.1961.tb02130.x.
[38] R.H. Stokes, R.A. Robinson, Standard solution for humidity control at 25°C, Ind Eng Chem. 41 (1949) 2013.
[39] J.J. Ayerdi, A. Aginagalde, I. Llavori, J. Bonse, D. Spaltmann, A. Zabala, Ball-on-flat linear reciprocating tests: Critical assessment of wear volume determination methods and suggested improvements for ASTM D7755 standard, Wear. 470–471 (2021) 203620. https://doi.org/10.1016/j.wear.2021.203620.
[40] C.D. Wagner, L.E. Davis, M.V. Zeller, J.A. Taylor, R.H. Raymond, L.H. Gale, Empirical atomic sensitivity factors for quantitative analysis by electron spectroscopy for chemical analysis, Surf. Interface Anal. 3 (1981) 211–225. https://doi.org/10.1002/sia.740030506.
[41] C.Y. Tam, C.H. Shek, W.H. Wang, Oxidation behaviour of a Cu-Zr-Al bulk metallic glass, Rev. Adv. Mater. Sci. 18 (2008) 107–111.
[42] X.P. Nie, X.H. Yang, L.Y. Chen, K.B. Yeap, K.Y. Zeng, D. Li, J.S. Pan, X.D. Wang, Q.P. Cao, S.Q. Ding, J.Z. Jiang, The effect of oxidation on the corrosion resistance and mechanical properties of a Zr-based metallic glass, Corros. Sci. 53 (2011) 3557–3565. https://doi.org/10.1016/j.corsci.2011.06.032.
[43] M. Kilo, M. Hund, G. Sauer, A. Baiker, A. Wokaun, Reaction induced surface segregation in amorphous CuZr, NiZr and PdZr alloys—an XPS and SIMS depth profiling study, J. Alloys Compd. 236 (1996) 137–150. https://doi.org/10.1016/0925-8388(95)02143-4.
[44] H.M. Kimura, K. Asami, A. Inoue, T. Masumoto, The oxidation of amorphous Zr-base binary alloys in air, Corros. Sci. 35 (1993) 909–915. https://doi.org/10.1016/0010-938X(93)90308-4.
[45] D.D. Hawn, B.M. DeKoven, Deconvolution as a correction for photoelectron inelastic energy losses in the core level XPS spectra of iron oxides, Surf. Interface Anal. 10 (1987) 63–74. https://doi.org/10.1002/sia.740100203.
[46] B. Prakash, K. Hiratsuka, Sliding wear behaviour of some Fe-, Co- and Ni-based metallic glasses during rubbing against bearing steel, Tribol. Lett. 8 (2000) 153–160. https://doi.org/10.1023/A:1019191303146.
[47] E.R. Leheup, R.E. Pendlebury, Unlubricated reciprocating wear of stainless steel with an interfacial air flow, Wear. 142 (1991) 351–372. https://doi.org/10.1016/0043-1648(91)90174-S.
[48] P. de Baets, G. Kalacska, K. Strijckmans, F. Van de Velde, A.P. Van Peteghem, Experimental study by means of thin layer activation of the humidity influence on the

fretting wear of steel surfaces, Wear. 216 (1998) 131–137. https://doi.org/10.1016/S0043-1648(97)00189-0.
[49] S. Yamamoto, O.T. Kendelewicz, J.T. Newberg, G. Ketteler, D.E. Starr, E.R. Mysak, K.J. Andersson, H. Ogasawara, H. Bluhm, M. Salmeron, G.E. Brown, A. Nilsson, Water Adsorption on r-Fe2O3(0001) at near Ambient Conditions SLAC-PUB-13827, (2009).
[50] S. Bhowmik, R. Naik, Selection of Abrasive Materials for Manufacturing Grinding Wheels, Mater. Today Proc. 5 (2018) 2860–2864. https://doi.org/10.1016/j.matpr.2018.01.077.
[51] D. Klaffke, On the repeatability of friction and wear results and on the influence of humidity in oscillating sliding tests of steel-steel pairings, Wear. 189 (1995) 117–121. https://doi.org/10.1016/0043-1648(95)06672-1.
[52] H.-K. Oh, K.-H. Yeon, H. Yun Kim, The influence of atmospheric humidity on the friction and wear of carbon steels, J. Mater. Process. Technol. 95 (1999) 10–16. https://doi.org/10.1016/S0924-0136(99)00259-9.

Authors biographies

Solène STOENS. She received her MSC degree in mechanical engineering at University of Technology of Compiègne (France) in 2020. She is performing her Ph.D. at Femto-ST Institute (France) since 2020. Her main interests concern the behavior of Bulk Metallic Glasses during tribological solicitations.

Rémi DAUDIN. He received his Ph.D. in condensed matter physics from the Grenoble University in 2012 for his studies on the metallic liquid structure at a liquid/solid interface. He continued with a three-years post-doc position at SIMaP laboratory in the field of in situ X-ray tomography during the solidification of metal-matrix nano-composites. After a one year position at Catholic University of Louvain on metallic glass thin films, he joined the SIMaP laboratory in 2017 where his main interests concern the relationship between the

structural state, the deformation mechanisms and the mechanical properties of metallic glasses.

Graphical abstract

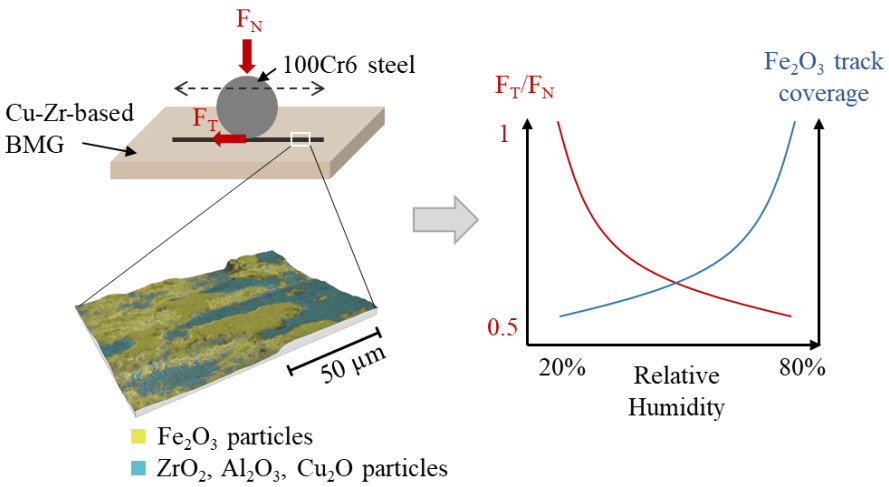

Supplementary Material

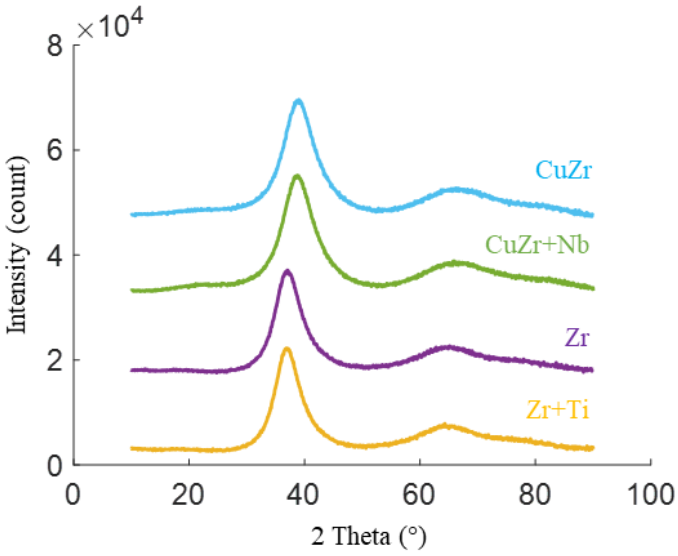

Figure S1 – XRD spectrums preformed on each BMG composition (CuZr, CuZr+Nb, Zr and Zr+Ti).

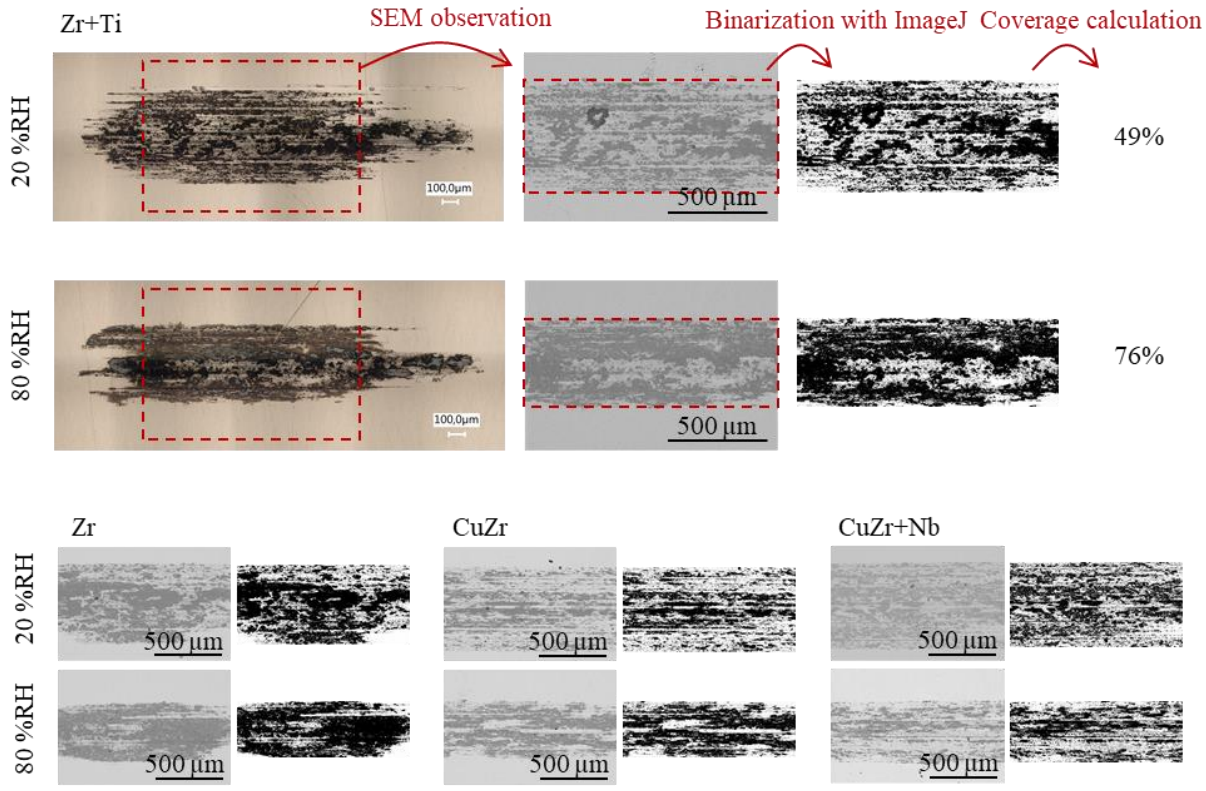

Figure S2 – Calculation of the 3rd-body coverage ratio based on SEM observations (BSE detector), post-treated with ImageJ.

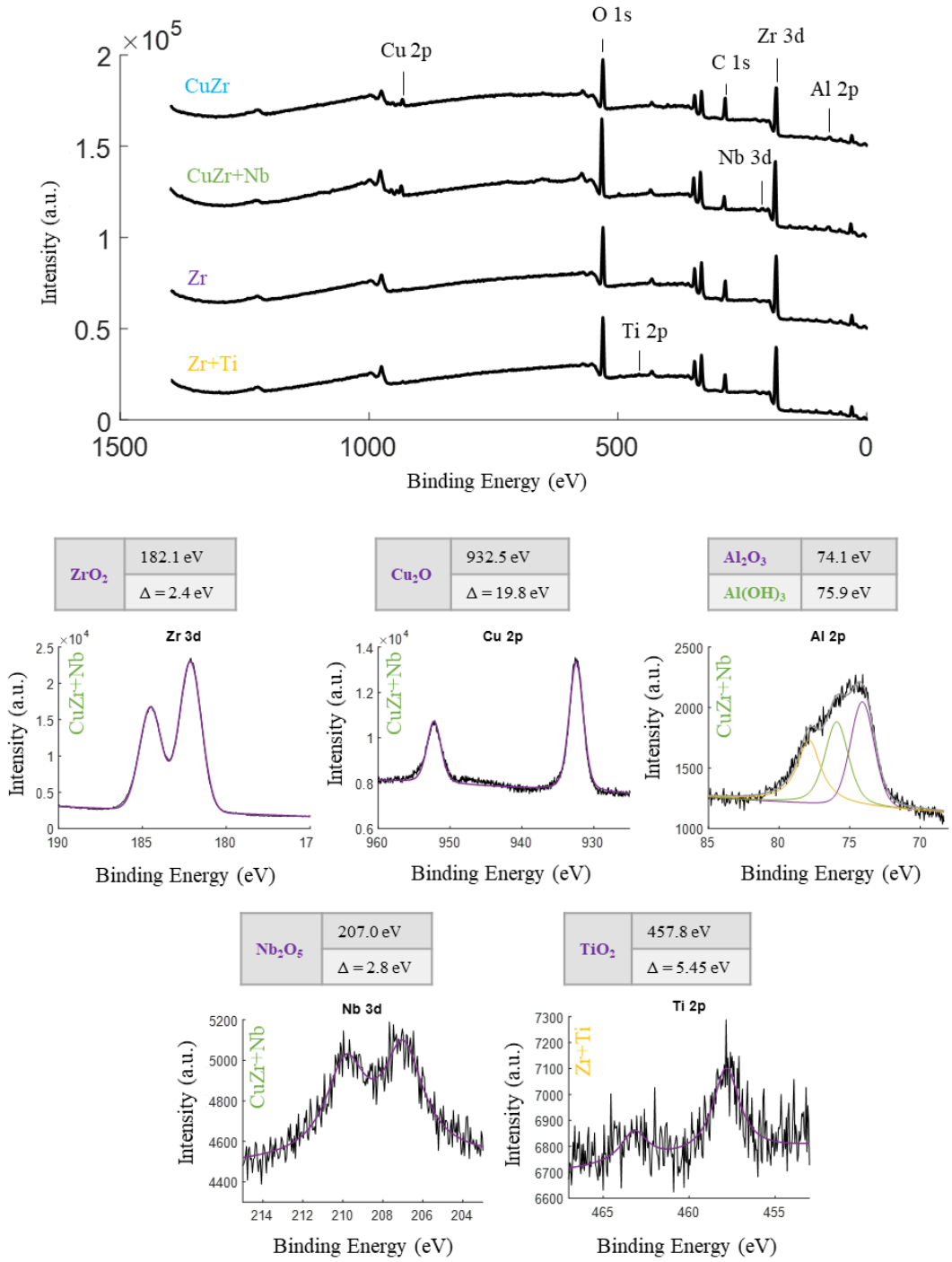

Figure S3 – XPS analyses performed on CuZr, CuZr+Nb, Zr and Zr+Ti raw surfaces after polishing and cleaning. Zr 3d, Cu 2p, Al 2p and Nb 3d peaks from CuZr+Nb sample. Ti 2p peak from Zr+Ti sample. Identified oxides are indicated above each spectrum with associated binding energy and splitting (Δ).

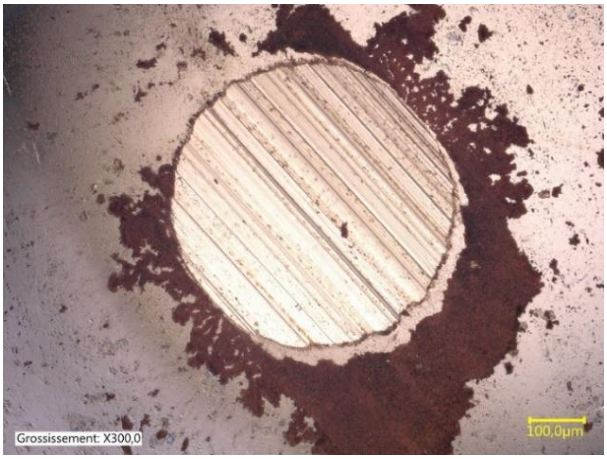

Figure S4 – Optical image of the wear track of a steel ball. Dark particles outside of the track are volatile particles.

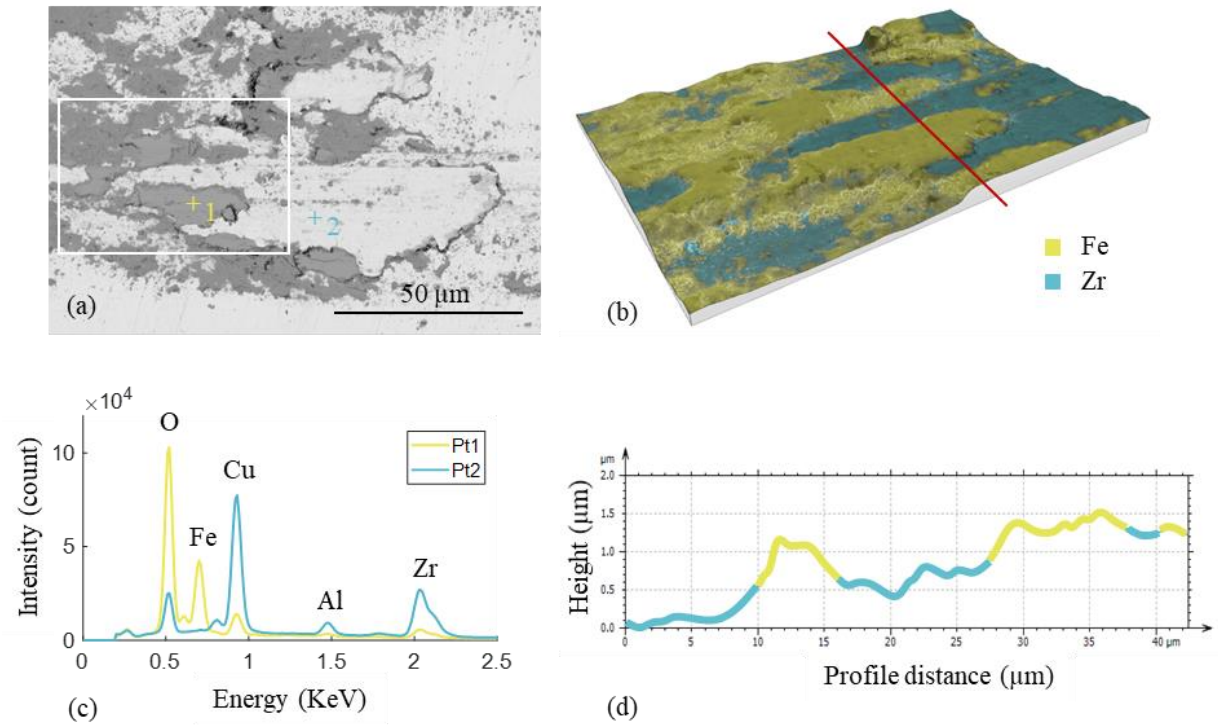

Figure S5 - SEM observation of a CuZr wear track at 60 %RH with BSE detector (a), combined representation of 3D-SEM image and EDS mapping of the white-framed area (b), EDS analyses carried out at point 1 and 2 (c), Height profile along the red line displayed on (b) obtained with Mountains® from Digital Surf (d).

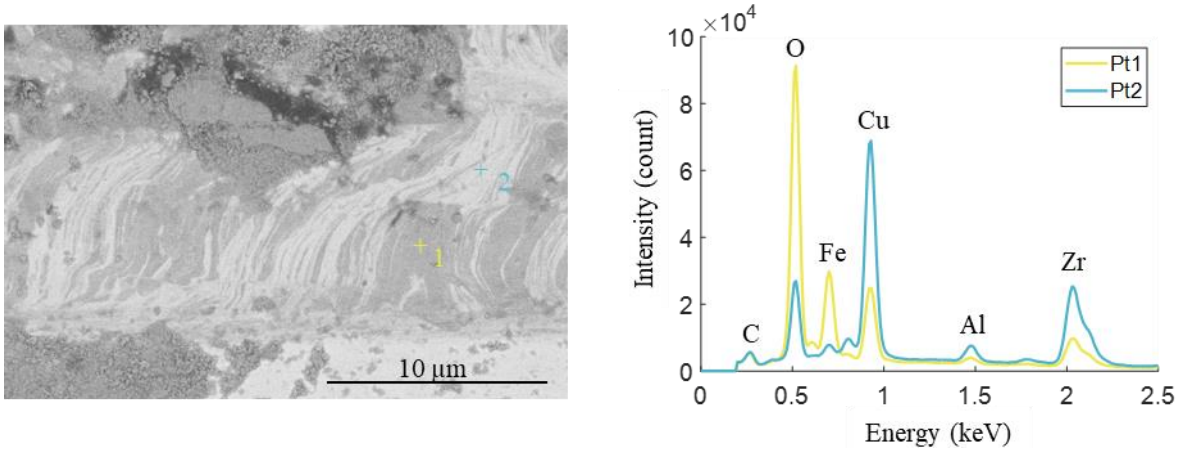

Figure S6 – SEM picture of a CuZr+Nb wear track at 20 %RH with BSE detector (left) and EDS analyses performed at points 1 and 2 (right).

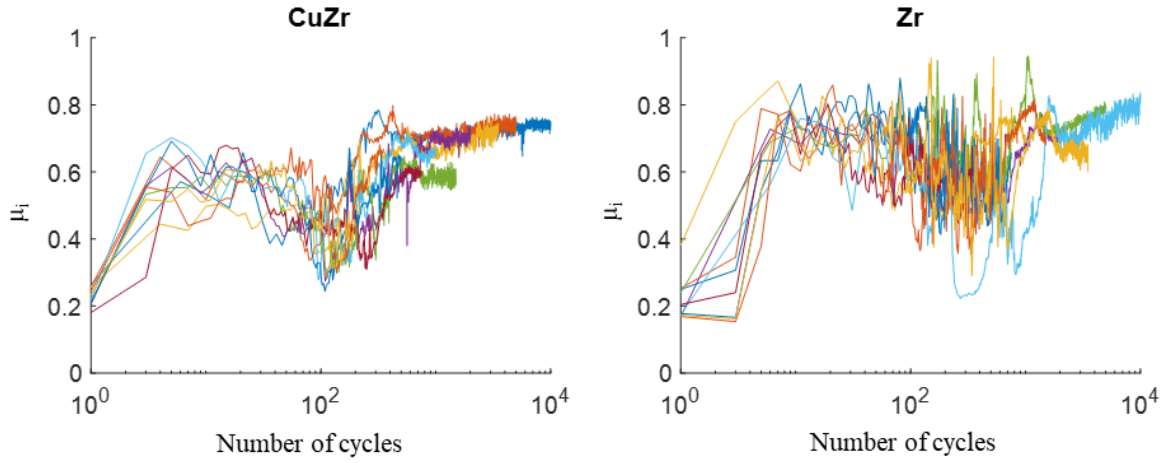

Figure S7 – μ_i against number of cycles with one test performed with each following number of cycles (N): 200 – 350 – 500 – 750 – 1,000 – 1,500 – 2,000 – 3,500 – 5,000 – 10,000. RH = 50 ± 1 %RH. F_N = 1 N.

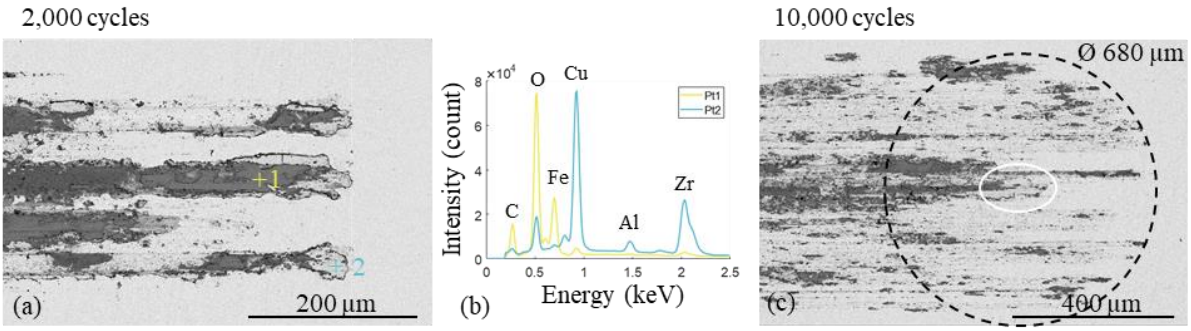

Figure S8 – SEM observations with BSE detector of the wear tracks extremities on the CuZr plate after a test of 2,000 friction cycles at 50 %RH (a) and after a test of 10,000 friction cycles at 50 %RH (c). The black dotted circle defines the contact area with the ball, whose diameter was measured on the wear track of the ball. The white circled area locates the white patch at extremity of the track. EDS analyses performed at points 1 and 2 (b).